ERK signaling dissolves ERF Repression Condensates in Living Embryos

Claire J. Weaver[a,b], Aleena L. Patel[a,b,,2], Stanislav Y. Shvartsman[a,b,c], Michael S. Levine[a,b,1], Nicholas Treen[a,1]

[a]Lewis-Sigler Institute for Integrative Genomics, Princeton University, Princeton, NJ 08544; [b]Department of Molecular Biology, Princeton University, Princeton, NJ 08544; [c]Flatiron Institute, Simons Foundation, New York, NY 10010.

Author contributions: N.T and M.S.L designed research with contributions from S.Y.S; N.T and C.J.W performed experiments; C.J.W and A.L.P analyzed data; N.T, M.S.L and C.J.P wrote the paper with contributions from S.Y.S and A.L.P.

[1]To whom correspondence may be addressed. Email: ntreen@princeton.edu (N.T) or msl2@princeton.edu (M.S.L)

[2]Present address: Department of Developmental Biology, Stanford Medicine, Stanford, CA, 94305

ABSTRACT

Phase separation underlies the organization of the nucleus, including the biogenesis of nucleoli and the packaging of heterochromatin. Here we explore the regulation of transcription factor condensates involved in gene repression by ERK signaling in gastrulating embryos of a simple proto-vertebrate (*Ciona*). ERK signaling induces nuclear export of the transcriptional repressor ERF, which has been linked to various human developmental disorders. Using high resolution imaging we show that ERF is localized within discrete nuclear condensates that dissolve upon ERK activation. Interestingly, we observe dynamic pulses of assembly and dissociation during the cell cycle, providing the first visualization of a nuclear phase separation process that is regulated by cell signaling. We discuss the implications of these observations for producing sharp on/off switches in gene activity and suppressing noise in cell-cell signaling events.

INTRODUCTION

Liquid-liquid phase separation (LLPS) is emerging as a major mechanism for cellular organization (1), including the biogenesis of nucleoli and other components of the nucleus (2, 3). Within nuclei, LLPS has also been implicated in the assembly of the RNA Polymerase II pre-initiation complex at poised promoters (4-6), as well transcriptional silencing. HP1 chromocenters display liquid behavior (7, 8), and the transcriptional repressor Hes.a was recently shown to possess liquid properties when associated with the Groucho (Gro/TLE) corepressor (9). Hes.a/Gro condensates are stable throughout the cell cycle when expressed in living *Ciona* embryos, finally dissolving at the onset of mitosis (9). These observations point towards a simple mechanism for transcriptional repression, whereby Hes.a/Gro condensates exclude transcriptional activators at silent loci (9).

Transcriptional repressors are often deployed to silence gene expression in the absence of cell signaling (10). This default repression is inhibited upon cell signaling to activate gene expression (10, 11). Here, we explore the possibility that cell signaling derepresses gene silencing by influencing the assembly and disassembly of repression condensates. In ERK signaling, the activation of a receptor by its ligand (e.g., FGF) triggers a phosphorylation cascade culminating in the activation and nuclear translocation of ERK (12). Previous studies suggest ERK signaling anagonizes transcriptional repressors such as Capicua, Yan and ERF (13-16), in addition to inducing the activities of transcriptional activators such as ETS and Pointed (17).

In the *Ciona* embryo, FGF/ERK signaling is pervasively used to specify a variety of cell types, including cardiomyocytes and neuronal cell types in the CNS (18-20). This signaling acts upon ETS-class transcription factors - typically interpreted as activators, although de-repression mechanisms are likely to participate as well. The maternally expressed *Ciona* orthologue of the human Ets-2 repressive factor (ERF) is a strong candidate for one such repressor as it persists throughout early development (21). Mammalian ERF is a sequence-specific repressor that recognizes canonical ETS binding sites (15, 22, 23) and is exported from the nucleus upon ERK activation (15, 23). It has been implicated in a variety of human diseases, including craniofacial disorders (24).

We present evidence that ERF forms spherical condensates during *Ciona* embryonic development, but FGF/ERK signaling leads to their dissolution and export from the nucleus. There is a tight correlation between the formation of ERF condensates, association with the Groucho corepressor, and transcriptional silencing of FGF/ERK target genes. Unexpectedly, ERF condensates exhibit

a pulse of dissolution and reformation during interphase, suggesting transient rather than sustained FGF/ERK signaling. We suggest that regulating the assembly and disassembly of ERF condensates suppresses noise and produces sharp, switch-like induction of gene expression.

RESULTS

A survey of the *Ciona* genome identified two putative orthologues of the human ERF repressor. One is maternally expressed in the *Ciona* embryo (Erf.b/KY.Chr4.757), while the other does not produce detectable transcripts until late larval stages (Erf.a/KY.Chr4.415). We focused our efforts on the maternal orthologue, hereafter called ERF.

Ciona ERF was fused to mNeongreen (mNg) and expressed in the embryonic ectoderm of gastrulating *Ciona* embryos using a *Sox1/2/3* regulatory sequence (Fig. 1A). Nuclear, punctate fluorescence is readily detected. Super-resolution confocal microscopy revealed punctate distributions of ERF evocative of Hes.a repression condensates (Fig. 1D, Fig. S1A). The corepressor for ERF has not been definitively identified, although there is evidence for potential interactions between human ERF and TLE5 (25). We observed colocalization of Gro (TLE) within ERF puncta (Fig. 1D), suggesting that Gro functions as a corepressor of ERF in the *Ciona* embryo.

Unlike Hes.a condensates, ERF was erratically distributed across different nuclei, which may be due to localized FGF signaling during embryonic development. To explore this possibility ERK was activated throughout the ectoderm using a variant of human MEK (CaMEK) that possesses greater constitutive activity than commonly used phosphomimetic variants (26). This experimental activation of MEK caused ERF to be excluded from all nuclei (Fig. 1B), demonstrating ERF

93 localization is dependent on ERK signaling. When treated with the MEK inhibitor U0126 ERF
94 nuclear exclusion is reversed and nuclear accumulation is restored (Fig. 1C).
95
96 Co-expression of CaMEK not only led to export of ERF from the nucleus, but also caused a loss
97 of ERF/Gro puncta (Fig. 1E). These puncta are restored upon addition of the U0126 inhibitor (Fig.
98 1F), suggesting that ERF/Gro complexes are specific targets of ERK signaling. By contrast,
99 activation or inhibition of ERK had no noticeable effect on Hes.a condensates (Fig. S1).
100
101 Human ERF has an N-terminal ETS DNA binding domain followed by a disordered domain. A
102 region of this disordered sequence (residues 472-530) is essential for repression (Fig. 2A, 15). The
103 *Ciona* homologue of ERF has a similar N-terminal ETS domain, but also contains an additional
104 139 amino acid (AA) residues in the C-terminus (Fig. 2B; see below). This region is less disordered
105 than its human counterpart (Fig. 2B). It was previously shown that mutations in the DNA binding
106 of Hes.a resulted in condensates exhibiting definitive liquid-like properties (9). We similarly
107 observe that a K83Q mutation in the ERF ETS domain forms fewer, larger puncta, that retain
108 association with Gro (Fig. 2C). This mutation mimics a human clinical variant associated with
109 craniosynostosis (24). The mutant condensates display similar responses to activated or inhibited
110 MEK as their wildtype counterparts (Fig. 2D, E), suggesting that responses to ERK signaling can
111 occur irrespective of DNA binding. They also exhibit fusions of individual puncta, consistent with
112 the formation of ERF/Gro repression condensates via LLPS (Fig. 2F, Supplemental Movie 1).
113
114 To identify a putative repression domain, we created a series of truncations of ERF. Removal of
115 the C-terminal 140 amino acid residues disrupted droplet formation, while loss of an additional 20

116 AA residues resulted in uniform distribution throughout the nucleus (Fig. S2A). This behavior is
117 similar to previous observations for Hes.a where the removal of the Gro-interaction motif
118 (WRPW) abolished droplet formation (9). Based on these observations we designate the C-
119 terminal 160 residues of Ci-ERF as a droplet forming domain (Fig. S2B).
120
121 We next asked whether this domain mediates repression. Chimeric proteins that replace the DNA
122 binding domain of human ERF with the DNA binding domains of other transcription factors were
123 found to retain ERK-modulated repression activities (15). We therefore replaced the ETS DNA
124 binding domain of *Ciona* ERF with the bHLH DNA binding domain of Hes.a (Fig. 3A). The
125 resulting chimera forms nuclear puncta (Fig. S3A), displays colocalization with Gro, and is
126 imported and exported from nuclei in response to experimental manipulation of MEK (Fig.
127 S3B,C). Removal of the 160 AA droplet domain from this chimeric protein resulted in a loss of
128 droplets and Gro colocalization (Fig. 3B-D).
129
130 The Hes.a/ERF chimera appears to repress a Hes.a target gene in response to FGF/ERK signaling.
131 The Hes.a target gene ZicL (27) is expressed in neuronal precursor cells of rows I-IV of the
132 presumptive neural plate (28). A reporter containing the upstream regulatory sequences of ZicL
133 recapitulates this localized pattern of expression (Fig. 3D, 20). Co-expression of CaMEK
134 throughout the early ectoderm results in an anterior expansion of the ZicL reporter gene (Fig. 3E').
135 Hes.a has previously been shown to repress this reporter (Fig. 3F, 9), and it continues to do so even
136 upon coexpression of CaMEK (Fig. 3F'). By contrast, the Hes.a/Erf chimera represses ZicL in the
137 neural plate, but not in posterior cells that are adjacent to a localized source of FGF/ERK signaling
138 (Fig. 3G, 29). Moreover, repression is completely abolished when CaMEK is expressed

throughout the neural plate (Fig.4G'). These observations suggest that the C-terminal 160 residues of the ERF protein are required for repression by recruiting Gro and derepression by FGF/ERK signaling (Fig. 3H).

Live imaging of gastrulating embryos revealed dynamic import and export of ERF from the nucleus over the course of a single interphase (Fig. 4A, S4, Supplemental Movies 2, 3). This behavior was variable, with some cells having ERF remain nuclear while others displayed complete exclusion from the nucleus throughout interphase (Supplemental Movies 2,3). ERF condensates were limited to ~500nm in diameter even upon complete inhibition of ERK signaling with U0126 (Fig. 4, Supplemental Supplemental Movies 4,5). Consistent with previously observed Hes.a condensate behaviors (9), the DNA-binding mutant formed fewer and larger droplets (Fig.S4, Supplemental Movies 4,). Pulsatile behavior was still observed, although the initial formation of condensates was short lived (Fig. S4, Supplemental Movies 6,7). When treated with U0126, mutant ERF condensates continued to grow and fuse to sizes over 1uM, considerably larger than wild-type condensates (Figs 4, S4, Supplemental Movies 8,9). These observations suggest that ERF condensate growth is limited by both DNA binding and ERK phosphorylation. This pulsatile behavior was never observed when embryos were treated with the U0126 inhibitor (Fig.4D), suggesting that nuclear export and dissolution is due to ERK signaling.

We observed that nuclear export is accompanied by a decrease in nuclear fluorescence and a concurrent increase in cytoplasmic fluorescence (Fig. 4 C). While nuclear fluorescence decreases, droplet number remains relatively unchanged for 3-5 mins. After this lag, there is a sudden and uniform dissolution of ERF/Gro condensates (Fig.4C, S3), suggesting ERK-mediated export

162 precedes dissolution. This behavior is not observed at mitosis, where the decrease in nuclear
163 florescence and dissolution of droplets were tightly correlated (Fig.4, S3). We discuss the
164 implications of these observations below.
165
166 **DISCUSSION**
167 We have presented evidence that ERF associates with Gro and forms repression condensates. This
168 association depends on an extended C-terminal region that is required for the recruitment of Gro,
169 the formation of condensates, and transcriptional repression. This differs from the short, dedicated
170 WRPW motif that mediates Hes.a-Gro associations, raising the possibility of distinct modes of
171 condensate formation for Hes.a and ERF. A particularly striking finding of our analysis is the
172 pulsatile assembly and dissolution of ERF/Gro condensates during the cell cycle. These dynamics
173 sharply contrast with the assembly of stable Hes.a condensates, highlighting the role of FGF/ERK
174 signaling in the precision of gene activity.
175
176 ERK signaling pathways often display oscillatory or pulsatile dynamics (30, 31). However, this
177 behavior was not anticipated for *Ciona* embryos since all signaling events, including FGF
178 signaling, is characterized by stable direct cell-cell contacts (18, 32, 33). Nonetheless, we observe
179 clear pulses of ERF/Gro assembly and disassembly during the cell cycle. These observations
180 suggest a short permissive period for response to ERK signaling during the cell cycle, despite
181 sustained cell-cell contacts. This restrictive period of response might suppress noise and help
182 ensure switch-like induction of gene activity by extracellular signals such as FGF.
183

Previous studies have implicated Ephrin is a key antagonist of FGF signaling in *Ciona* (34,35), raising the possibility that Ephrin inhibition works in concert with LLPS to ensure transcriptional precision. We note, however, that Ephrin activities are mainly detected at different stages of development than those examined in this study. Future studies will explore the relative roles of LLPS and Ephrin in the control of gene activity by FGF and other mediators of ERK signaling.

How does ERK signaling trigger the dissociation of ERF/Gro condensates? We tested the possibility that it might be due to ERF nuclear export. The idea is that export would trigger a domino effect, whereby ERF in the condensed phase would be released to compensate for reduced concentrations of ERF in the dilute phase. To test this idea we treated embryos with Leptomycin B, a drug shown to inhibit export of mammalian ERF (23). ERF/Gro condensates appear to dissolve on schedule despite this block in ERF nuclear export (Fig.S6). These observations are consistent with fast de-repression of genes in the *Drosophila* embryo, which occurs before ERK signals lead to nuclear export of the Capicua repressor (13, 36).

We therefore suggest that ERK-mediated phosphorylation underlies the dissolution of ERF repression condensates (Fig.5). It remains to be determined whether this phosphorylation occurs in the dilute phase, the condensed phase, or both. Regardless of mechanism, the dissolution of repression condensates is an inherently effective mechanism for the rapid, switch-like induction of gene expression in response to cell-cell signaling. It seems likely that a similar strategy is used for a variety of developmental patterning processes.

Figure 1

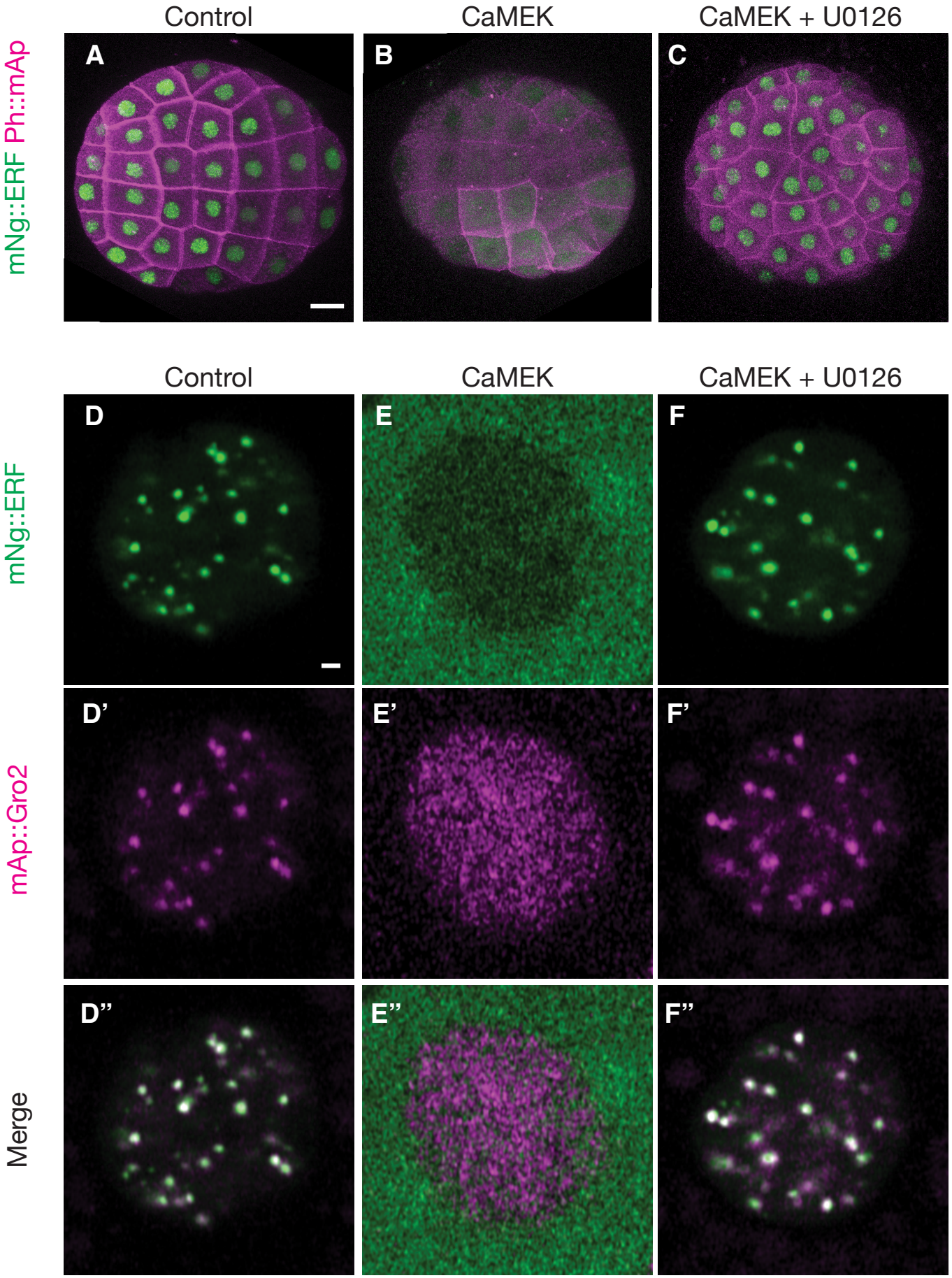
Control
CaMEK
CaMEK + U0126
mNg::ERF Ph::mAp
A
B
C
Control
CaMEK
CaMEK + U0126
mNg::ERF
D
E
F
mAp::Gro2
D'
E'
F'
Merge
D"
E"
F"

Fig. 1. ERF Nuclear export is dependent on ERK phosphorylation

All Figs show ectodermal cells of 110-cell stage expressing electroporated transgenes of fluorescent fusion proteins in ectodermal cells. (A-C) Whole embryo views of live *Ciona* embryos with the indicated experimental treatments. Cell outlines are visualized using PH::mAp. (A) mNg::ERF is localized to the nucleus. Levels of nuclear fluorescence was variable between nuclei. (B) CaMEK overexpression causes ERF to localize outside the nucleus. (C) Treatment of CaMEK overexpressed embryos with the MEK inhibitor U0126 reverses the action of CaMEK and nuclear localization of ERF is restored. (D-F) Confocal sections of single *Ciona* nuclei. mNg::ERF is localized to spherical puncta that colocalize with mAp::Gro2. Ng::ERF is exported to from the nucleus, but mAp::Gro2 remains nuclear when CaMEK is overexpressed. This action is reversed when treated with the MEK inhibitor U0126. Scale bars A: 20 μm, D: 1 μm.

Figure 2

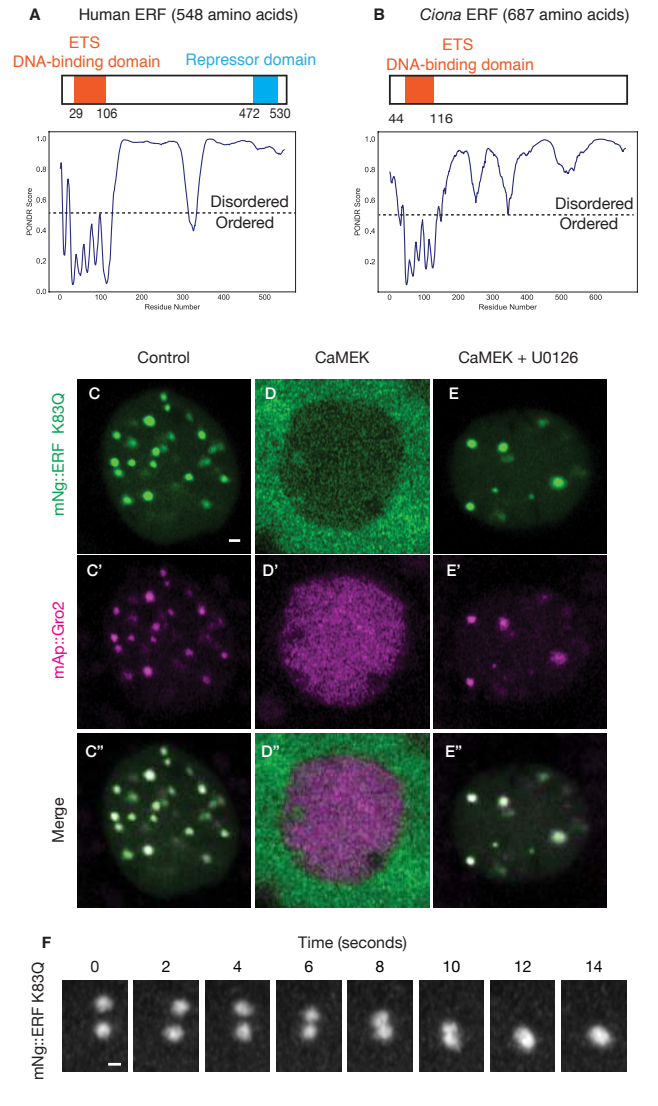
A
Human ERF (548 amino acids)
ETS
DNA-binding domain
Repressor domain
29
106
472
530
PONDR Score
Disordered
Ordered
Residue Number
B
Ciona ERF (687 amino acids)
ETS
DNA-binding domain
44
116
PONDR Score
Disordered
Ordered
Residue Number
Control
CaMEK
CaMEK + U0126
mNg::ERF K83Q
mAp::Gro2
Merge
C
D
E
C'
D'
E'
C"
D"
E"
F
Time (seconds)
0
2
4
6
8
10
12
14
mNg::ERF K83Q

Fig. 2. ERF DNA-binding mutants show liquid properties

(A,B) Primary structures of Human and Ciona ERF showing the ETS DNA-binding domain in orange and the repressor domain in blue. Below the structures are PONDR plots showing the predicted ordered and disordered regions. (C-E) Confocal sections of single *Ciona* nuclei. mNg::ERF K83Q is localized to spherical puncta that colocalize with mAp::Gro2. Ng::ERF K83Q is exported to from the nucleus, but mAp::Gro2 remains nuclear when CaMEK is overexpressed. This action is reversed when treated with the MEK inhibitor U0126. (F) Maximum intensity confocal projection showing the fusion of 2 Ng::ERF K83Q droplets over 14 seconds. Scale bars C: 10 μm, D: 0.5 μm.

Figure 3

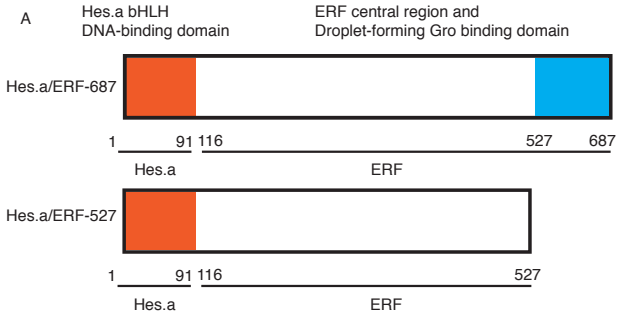
A
Hes.a bHLH
DNA-binding domain
ERF central region and
Droplet-forming Gro binding domain
Hes.a/ERF-687
1
91
116
527
687
Hes.a
ERF
Hes.a/ERF-527
1
91
116
527
Hes.a
ERF

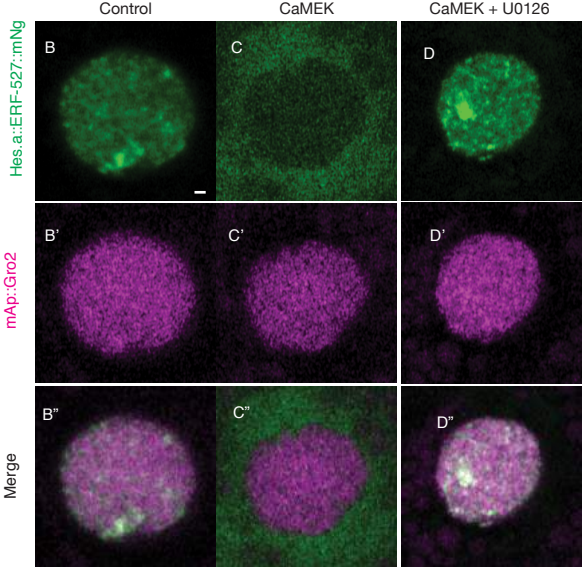
Control
CaMEK
CaMEK + U0126
Hes.a::ERF-527::mNg
mAp::Gro2
Merge
B
C
D
B'
C'
D'
B"
C"
D"

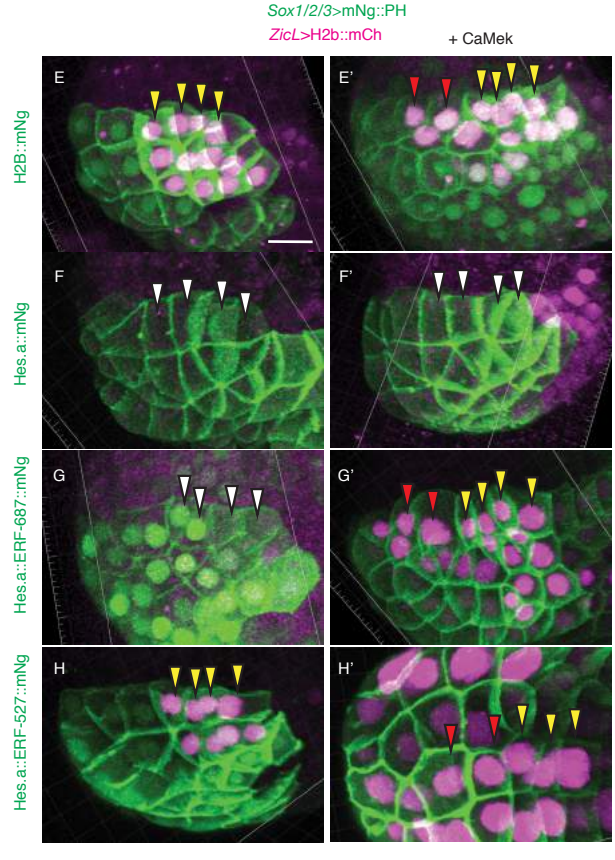
Sox1/2/3>mNg::PH
ZicL>H2b::mCh
+ CaMek
H2B::mNg
Hes.a::mNg
Hes.a::ERF-687::mNg
Hes.a::ERF-527::mNg
E
E'
F
F'
G
G'
H
H'

Fig. 3. *Ciona* ERF contains a C-terminal repressor domain

(A) Primary structures of Hes.a/ERF chimera proteins with the DNA binding and droplet froming domains indicated. (B-D) Confocal sections of single *Ciona* nuclei. Hes.a::ERF-527::mNg is localized to puncta that do not colocalize with mAp::Gro2. Hes.a::ERF-527:mNG is exported to from the nucleus, but mAp::Gro2 remains nuclear when CaMEK is overexpressed. This action is reversed when treated with the MEK inhibitor U0126. (E,E') Expression of ZicL reporter in the *Ciona* neural plate is expanded anteriorly when CaMEK is expressed. (F,F') Hes.a::mNG represses all ZicL expression in the neural plate. (G,G') Hes.a::ERF-687::mNG represses ZicL. This repression is inactivated by CaMEK. (H,H') Hes.a::ERF-527::mNg is unable to repress ZicL. Yellow arrowheads indicate Wild type expression. Red arrowheads indicate ectopic expression, white arrowheads indicate repression of wild type expression. Cell outlines are indicated with Ph::mNG as in several cases the transcription factors of interest are degraded by the time reporter activity is detectable. Scale bars A: 1 μm, E: 015 μm.

Figure 4

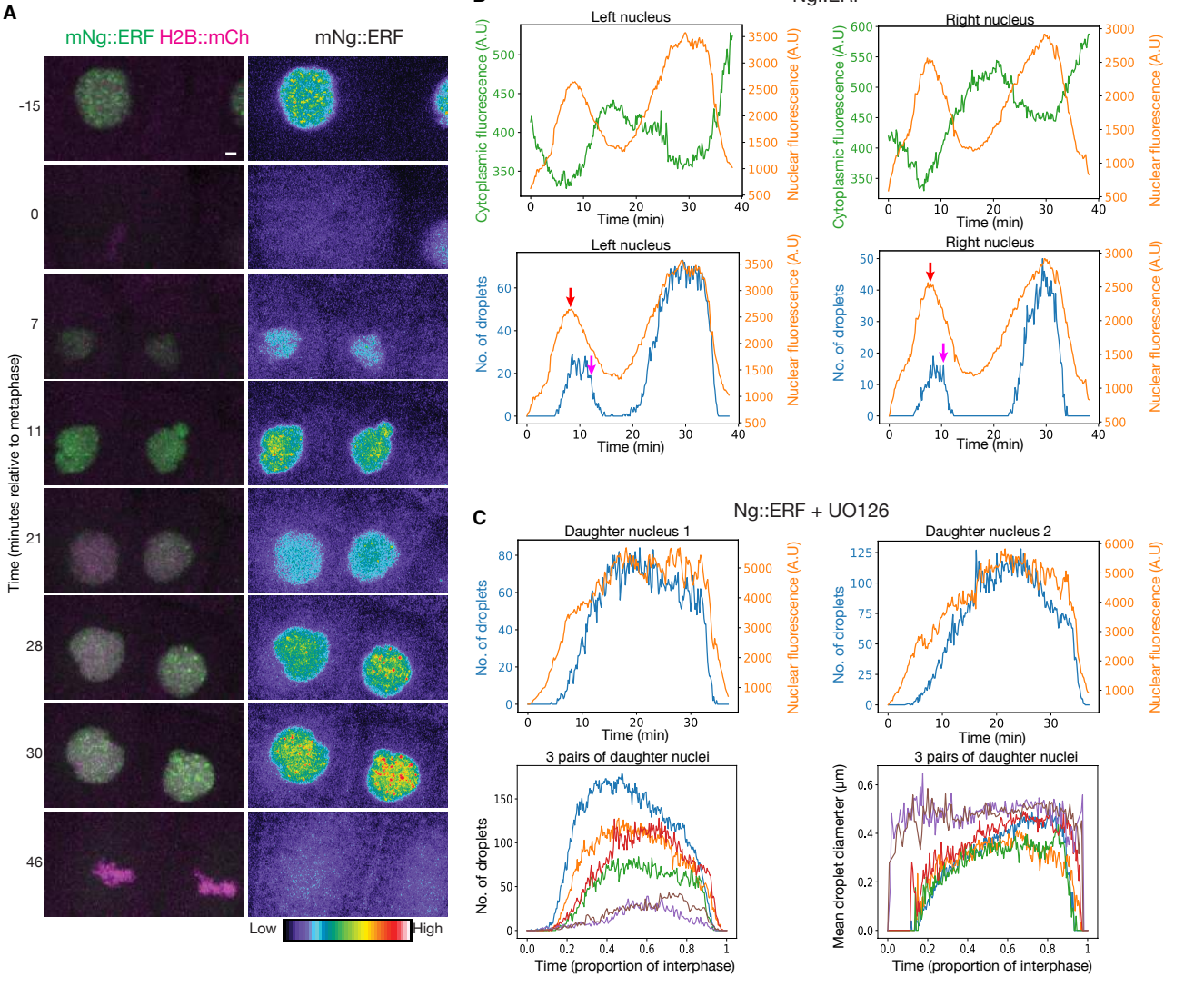
A
mNg::ERF H2B::mCh
mNg::ERF
-15
0
7
11
21
28
30
46
Time (minutes relative to metaphase)
Low
High
B
Ng::ERF
Left nucleus
Right nucleus
Cytoplasmic fluorescence (A.U)
Nuclear fluorescence (A.U)
Time (min)
No. of droplets
C
Ng::ERF + UO126
Daughter nucleus 1
Daughter nucleus 2
3 pairs of daughter nuclei
Time (proportion of interphase)
Mean droplet diamerter (µm)

Fig. 4. ERF pulses during interphase

(A,B) Maximum intensity confocal projection of a *Ciona* nucleus dividing and the daughter cells throughout interphase. Ng::ERF is exported and imported from the nucleus throughout interphase. (C) Quantifications of the nuclear fluorescence intensity, number of droplets, and cytoplasmic fluorescence intensity of the daughter nuclei in A and B. Red arrowheads indicate the approximate time that nuclear fluorescence intensity decreases and yellow arrowheads indicate the approximate time that number of droplets abruptly decreases. Scale bar: 1 μm.

Figure 5

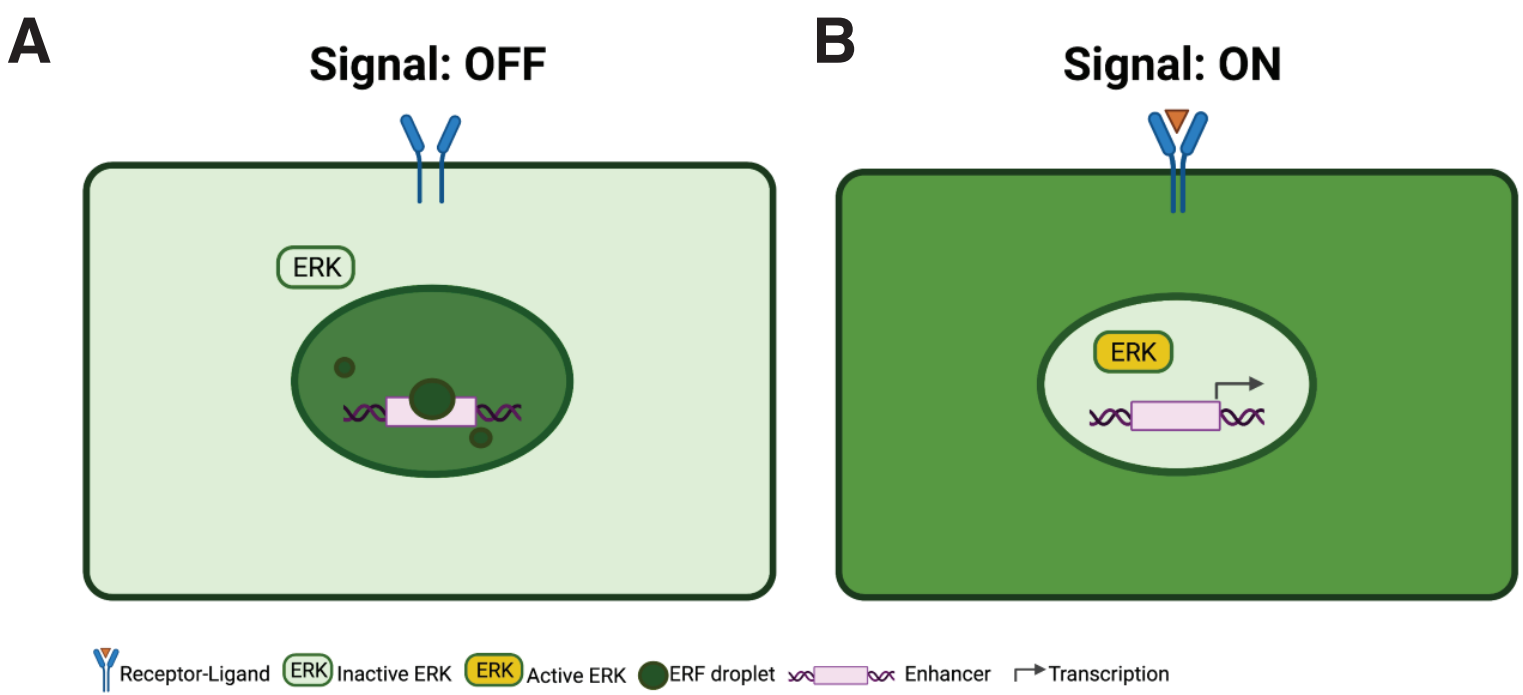
A
Signal: OFF
ERK
B
Signal: ON
ERK
Receptor-Ligand
ERK
Inactive ERK
ERK
Active ERK
ERF droplet
Enhancer
Transcription

Fig. 5. ERF derepression by dissolution of repressive condensates

(A) In the absence of an inductive signal ERK is inactive and ERF is localized to the nucleus where it forms repressive condensates as well as a dilute phase. (B) When a signal is activated, ERK enters the nucleus and will immediately phosphorylate ERF, causing it to be exported from the nucleus and for repressive condensates to dissolve. After an extended or intense period of signaling the repressive condensates will dissolve and transcriptional activation can proceed.

Figure S1

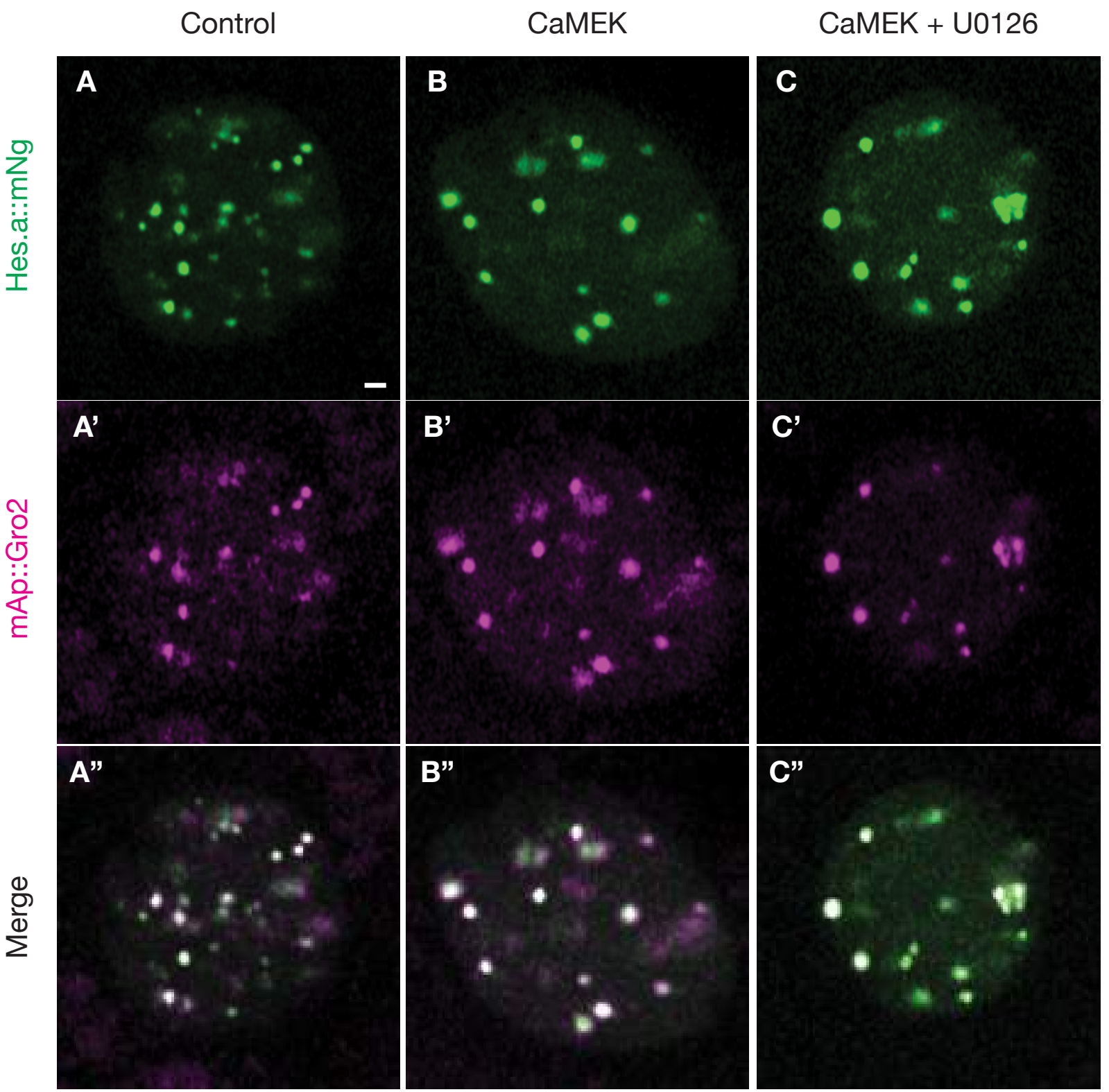
Control
CaMEK
CaMEK + U0126
Hes.a::mNg
mAp::Gro2
Merge
A
B
C
A'
B'
C'
A"
B"
C"

Supplementary Fig. 1. Hes.a does not respond to ERK activity

(A-C) Confocal sections of single *Ciona* nuclei. Hes.a::Ng is distributed in spherical puncta that colocalize with mAp::Gro2 in all conditions. Scale bar: 1 μm.

Figure S2

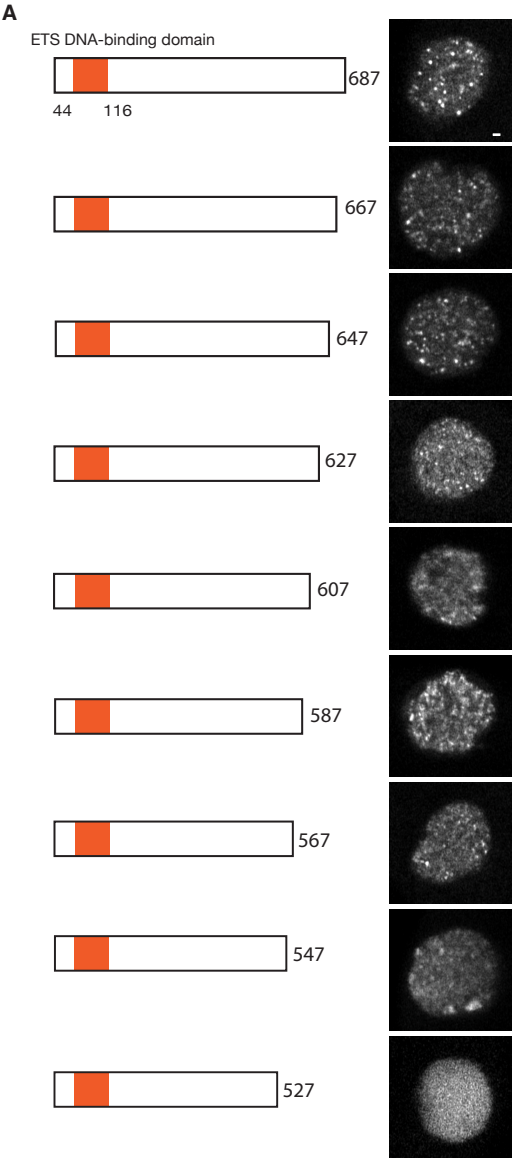
A
ETS DNA-binding domain
687
44
116
667
647
627
607
587
567
547
527
B
ETS DNA-binding domain
Droplet-forming domain
44
116
527
687

Supplementary Fig. 2. The C-terminus of ERF is a droplet forming domain

(A) Primary structure of *Ciona* truncated ERF showing the ETS DNA-binding domain in orange and indicating the total length of the protein. Corresponding images show confocal sections of single *Ciona* nuclei expressing the truncated form of ERF. Some droplet formation can be seen until 160 C-terminal residues are removed. (B) Primary structure of *Ciona* ERF showing the ETS DNA-binding domain in orange and the droplet forming domain in blue. Scale bar: 1 μm.

Figure S3

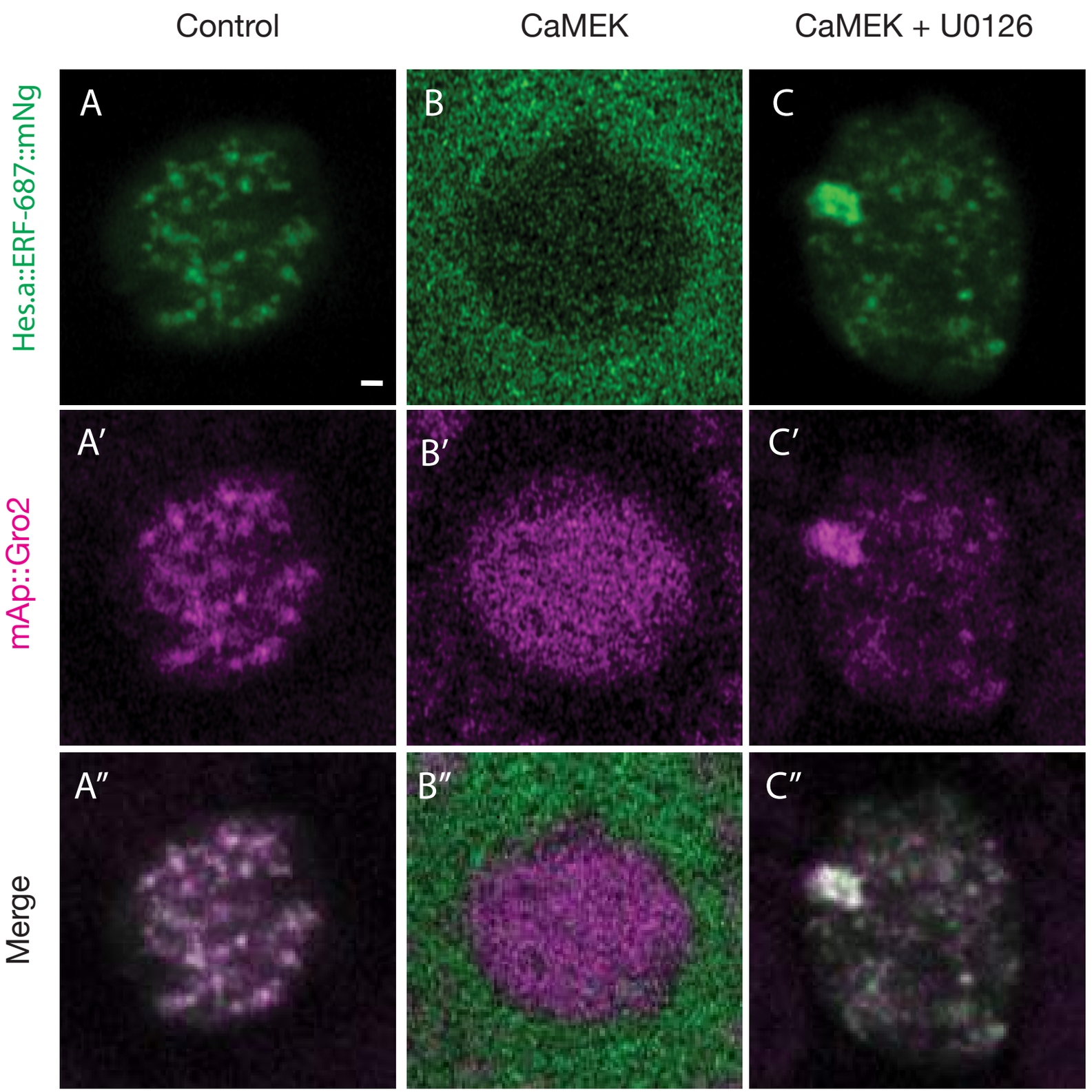
Control
CaMEK
CaMEK + U0126
Hes.a::ERF-687::mNg
mAp::Gro2
Merge
A
B
C
A′
B′
C′
A″
B″
C″

Supplementary Fig. 3. A Hes.a-ERF fusion shows droplet-like distribution and ERK phosphorylation dependent nuclear export.

(A-C) Confocal sections of single *Ciona* nuclei. Hes.a::ERF-687::mNg is localized to puncta that colocalize with mAp::Gro2. Hes.a::ERF-687:mNG is exported to from the nucleus, but mAp::Gro2 remains nuclear when CaMEK is overexpressed. Treatment with U0126 restores nuclear localization and puncta formation. Scale bar: 1 μm.

Figure S4

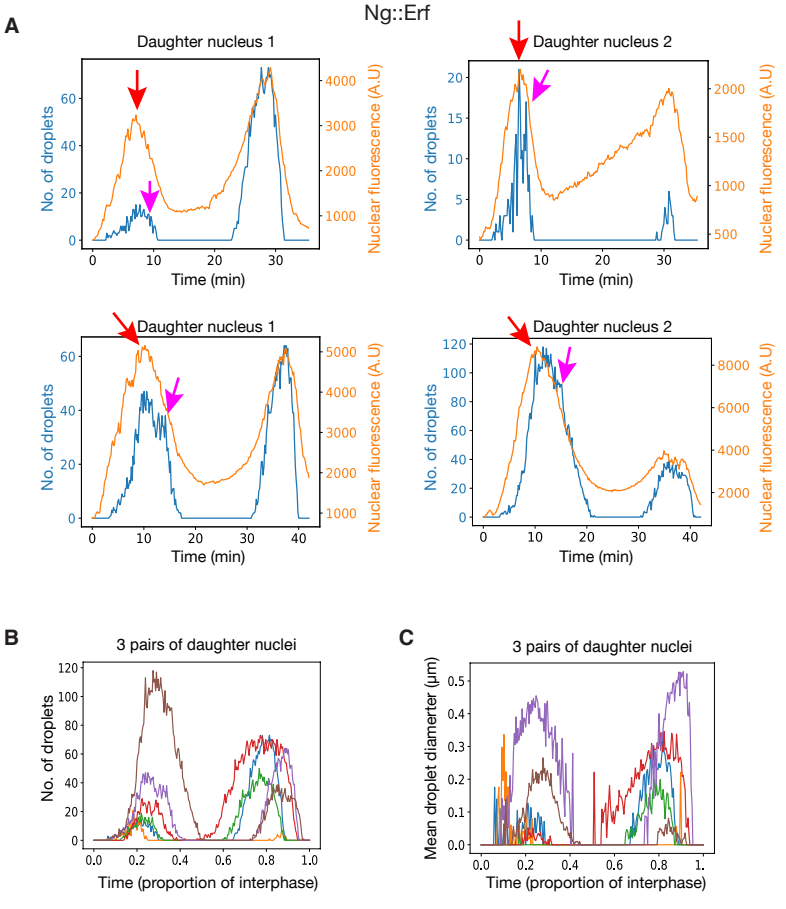
A
Ng::Erf
Daughter nucleus 1
Daughter nucleus 2
Daughter nucleus 1
Daughter nucleus 2
No. of droplets
Nuclear fluorescence (A.U)
Time (min)
B
3 pairs of daughter nuclei
No. of droplets
Time (proportion of interphase)
C
3 pairs of daughter nuclei
Mean droplet diamerter (µm)
Time (proportion of interphase)

Supplementary Fig. 4. Additional examples of ERF pulses during interphase

(A) Quantifications of the Ng::ERF nuclear fluorescence intensity and number of droplets intensity of 2 pairs of sister nuclei. Red arrows indicate the approximate time that nuclear fluorescence intensity decreases, and magenta arrows indicate the approximate time that number of droplets abruptly decreases. (B) Quantifications of number of Ng::ERF droplets from the 6 nuclei in (A) and Fig. 4B. Time is normalized to the relative proportion of interphase. (C)

Figure S5

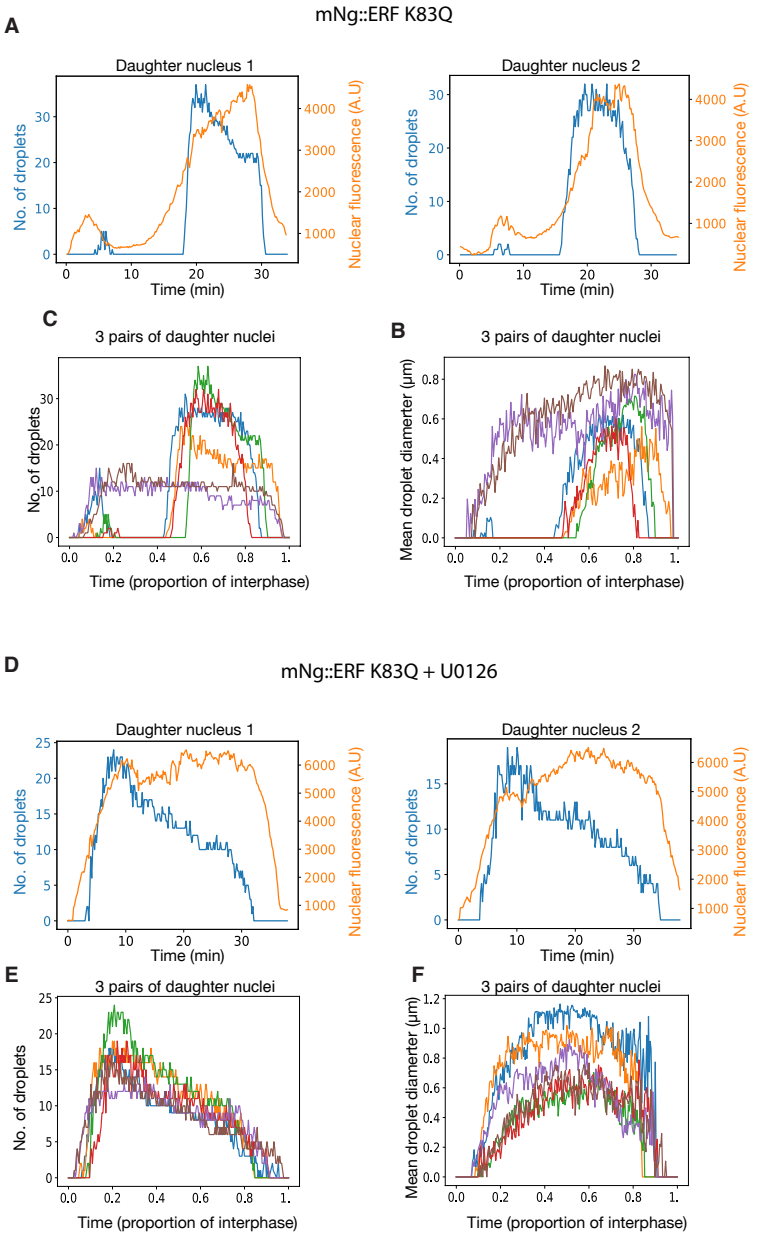
A
mNg::ERF K83Q
Daughter nucleus 1
Daughter nucleus 2
No. of droplets
Nuclear fluorescence (A.U)
Time (min)
C
3 pairs of daughter nuclei
No. of droplets
Time (proportion of interphase)
B
3 pairs of daughter nuclei
Mean droplet diameter (µm)
Time (proportion of interphase)
D
mNg::ERF K83Q + U0126
Daughter nucleus 1
Daughter nucleus 2
No. of droplets
Nuclear fluorescence (A.U)
Time (min)
E
3 pairs of daughter nuclei
No. of droplets
Time (proportion of interphase)
F
3 pairs of daughter nuclei
Mean droplet diameter (µm)
Time (proportion of interphase)

Supplementary Fig. 5. Mutant ERF shows altered droplet behaviors

(A) Quantifications of the Ng::ERF K83Q mutant nuclear fluorescence intensity and number of droplets intensity for a pair of sister nuclei. (B) Quantifications of the number of droplets for the Ng::ERF K83Q mutant in 6 pairs of sister nuclei including the pair shown in A. (C) Quantifications of the mean droplet diameter for the Ng::ERF K83Q mutant in 6 pairs of sister nuclei including the pair shown in A. (D-F) The same conditions as A-C but experiments were performed in the presence of the inhibitor U0126.

Figure S6

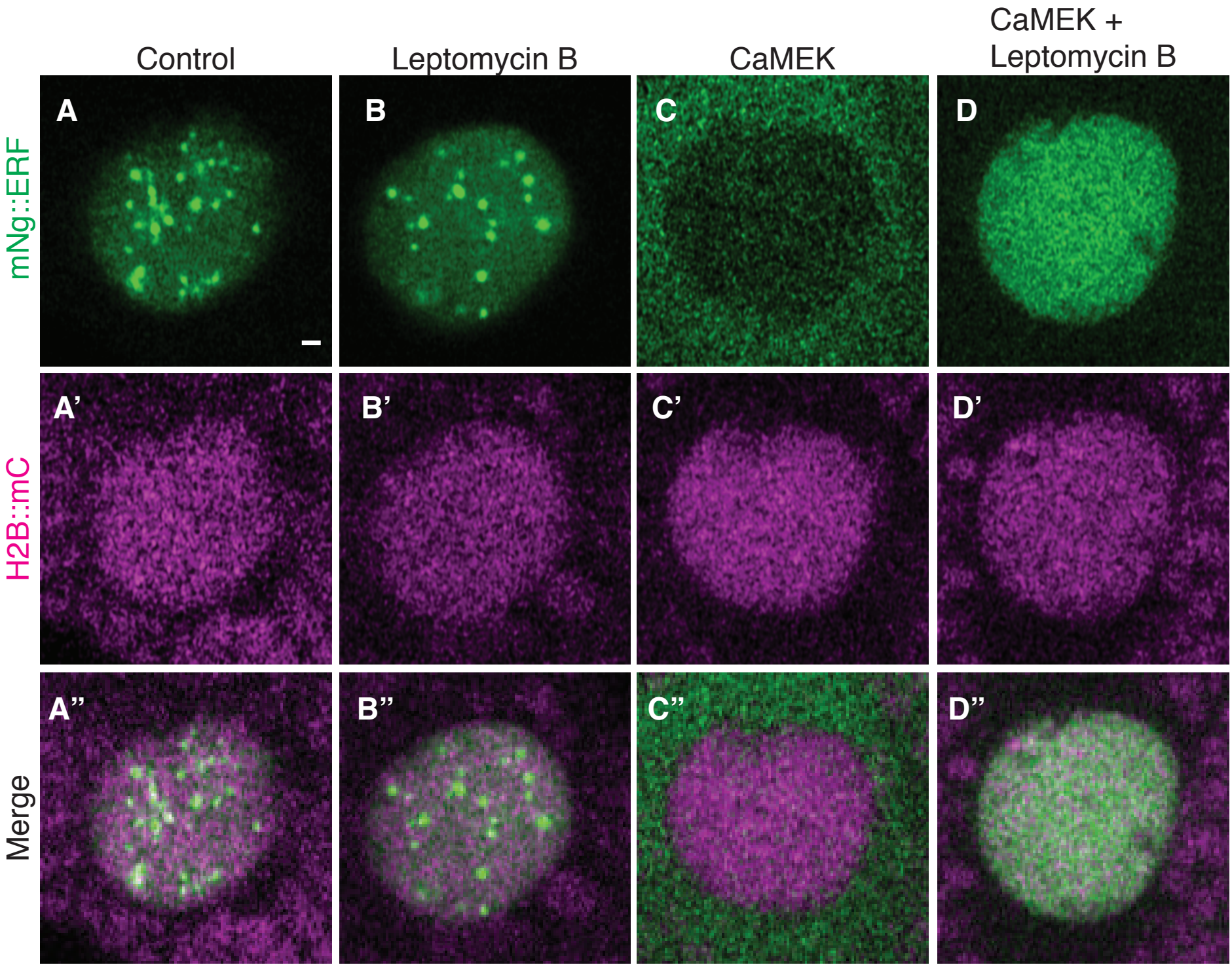
Control
Leptomycin B
CaMEK
CaMEK +
Leptomycin B
mNg::ERF
H2B::mC
Merge
A
B
C
D
A'
B'
C'
D'
A"
B"
C"
D"

Supplementary Fig. 6. ERF droplets do not require nuclear export to dissolve

(A-D) Confocal sections of single *Ciona* nuclei expressing Ng::ERF and H2B::mC. (A) control embryos show nuclear droplets. (B) ERF Droplets persist when embryos are treated with LeptomycinB. (C) ERF Droplets dissolve and ERF is exported from the nucleus when MEK is activated. (D) Nuclear ERF is recovered, but droplets do not form when MEK is activated and embryos are treated with Leptomycin B. Scale bar: 1 μm.

Supplementary movie 1. Fusion of mNg::ERF K83Q droplets.

Supplementary movie 2. mNG::ERF in living *Ciona* embryos.

Supplementary movie 3. 3 separate mitoses depicting mNG::ERF pulses in living *Ciona* embryos.

Supplementary movie 4. mNG::ERF in living *Ciona* embryos treated with U0126.

Supplementary movie 5. A single mitosis depicting mNG::ERF in living *Ciona* embryos treated with U0126.

Supplementary movie 6 mNg::ERF K83Q DNA binding mutant in living *Ciona* embryos.

Supplementary movie 7. A single mitosis depicting mNG::ERF K83Q DNA binding mutant in living *Ciona* embryos.

Supplementary movie 8 mNg::ERF K83Q DNA binding mutant in living *Ciona* embryos treated with U0126.

Supplementary movie 9. A single mitosis depicting mNG::ERF K83Q DNA binding mutant in living *Ciona* embryos treated with U0126.

METHODS

Animals

Wild *Ciona intestinalis* (Pacific populations, Type A, also referred to as *Ciona robusta*) adults were commercially sourced from San Diego County, Ca by M-Rep. Animals were kept in aerated artificial seawater at 18°C. U0126 treatment concentration was 8 µM, Leptomycin B treatment concentration was 0.2 µM. Control embryos were treated with either 0.1% DMSO or ethanol.

Molecular Cloning

All novel plasmids constructed for this study were based on the *pSP Sox1/2/3>* plasmid previously described (9) with the open reading frames replaced by PCR amplifications using a proofreading DNA polymerase (Primestar, Takara) and plasmids were assembled from linear PCR products using NEBuilder HiFi DNA Assembly Master Mix (New England Biolabs). Full plasmid sequences and descriptions of the individual cloning steps can be provided upon request. The *ZicL>H2B::mCherry* plasmid has previously been described (29). The constitutively active variant of Human MEK has been previously described (26).

Electroporations

Dechorionated *Ciona* zygotes were electroporated as previously described (9). All experiments were replicated at least in triplicate using different batches of *Ciona* eggs.

Imaging

Imaging was performed as previously described (9) using a Zeiss 880 Confocal microscope equipped with an Airyscan detector in fast mode. Exact settings and raw imaging files are available upon request.

Image Analysis

All images were Airyscan processed using Zeiss Zen software (ZEN Version 2.3 and 2.6, Zeiss) The identification and quantification of droplets from confocal images were performed using the *Imaris* spot detection function. All conditions were quantified using the green fluorescence channel across all conditions. Estimated sizes of droplets ranged from 0.2-0.3 um (WT and mutant ERF) and 0.5 um (inhibitor treatments). Background subtraction and region growing were accounted for throughout the cell cycle to accurately report droplet quantity and size. Droplet number in Imaris was filtered using the quality filter and setting a droplet threshold of 95% to prevent false droplet identification. The absolute intensity was used to determine spot regions/diameter. All statistics were exported from Imaris. Further processing was done in Python to fill in the info for frames without droplets as containing 0 droplets of diameter 0. All values exactly equal to the cutoff were excluded from further analysis. The remaining values were normalized to cell cycle length and plotted using matplotlib.

Nuclear and cytoplasmic fluorescence quantification of Ng::ERF was performed in Fiji. A nuclear and cytoplasmic mask was defined and average fluorescence intensities were recorded. Data was plotted alongside droplet data using matplotlib.

ACKNOWLEDGEMENTS

We thank Clifford Brangwynne, Ned Wingreen and members of the Levine and Brangwynne labs for helpful discussions. We thank Chris Killen for video editing. This research was funded by an NIH grant (NS076542) to M.S.L. N.T is funded by a Princeton Catalysis Initiative grant. C.J.W. is funded by a National Science Foundation graduate research fellowship

References

1. A. A. Hyman, C. A. Weber, F. Jülicher, Liquid-liquid phase separation in biology. *Annu. Rev. Cell Dev. Biol.* **30**, 39–58 (2014).

2. A. R. Strom, C. P. Brangwynne, The liquid nucleome – phase transitions in the nucleus at a glance. *J. Cell Sci.* **132**, 1–7 (2019).

3. C. P. Brangwynne, T. J. Mitchison, A. A. Hyman, Active liquid-like behavior of nucleoli determines their size and shape in Xenopus laevis oocytes. *Proc. Natl. Acad. Sci. U. S. A.* **108**, 4334–4339 (2011).

4. W. K. Cho, *et al.*, Mediator and RNA polymerase II clusters associate in transcription-dependent condensates. *Science.* **361**, 412–415 (2018).

5. B. R. Sabari, *et al.*, Coactivator condensation at super-enhancers links phase separation and gene control. *Science.* **361**, eaar3958 (2018).

6. A. Boija, *et al.*, Transcription Factors Activate Genes through the Phase-Separation Capacity of Their Activation Domains. *Cell* **175**, 1842-1855.e16 (2018).

7. A. G. Larson, *et al.*, Liquid droplet formation by HP1α suggests a role for phase separation in heterochromatin. *Nature* **547**, 236–240 (2017).

8. A. R. Strom, *et al.*, Phase separation drives heterochromatin domain formation. *Nature* **547**, 241–245 (2017).

527 9. N. Treen, S. F. Shimobayashi, J. Eeftens, C. P. Brangwynne, M. Levine, Properties of
528 repression condensates in living Ciona embryos. *Nat. Commun.* **12**, 1–9 (2021).
529 10. S. Barolo, J. W. Posakony, Three habits of highly effective signaling pathways: Principles
530 of transcriptional control by developmental cell signaling. *Genes Dev.* **16**, 1167–1181 (2002).
531 11. M. Affolter, G. Pyrowolakis, A. Weiss, K. Basler, Signal-Induced Repression: The
532 Exception or the Rule in Developmental Signaling? *Dev. Cell* **15**, 11–22 (2008).
533 12. A. L. Patel, S. Y. Shvartsman, Outstanding questions in developmental ERK signaling.
534 *Dev.* **145** (2018).
535 13. G. Jiménez, S. Y. Shvartsman, Z. Paroush, The Capicua repressor - A general sensor of
536 RTK signaling in development and disease. *J. Cell Sci.* **125**, 1383–1391 (2012).
537 14. E. M. O'Neill, I. Rebay, R. Tjian, G. M. Rubin, The activities of two Ets-related
538 transcription factors required for drosophila eye development are modulated by the Ras/MAPK
539 pathway. *Cell* **78**, 137–147 (1994).
540 15. D. N. Sgouras, *et al.*, ERF: An ETS domain protein with strong transcriptional repressor
541 activity, can suppress ets-associated tumorigenesis and is regulated by phosphorylation during cell
542 cycle and mitogenic stimulation. *EMBO J.* **14**, 4781–4793 (1995).
543 16. G. Mavrothalassitis, J. Ghysdael, Proteins of the ETS family with transcriptional repressor
544 activity. *Oncogene* **19**, 6524–6532 (2000).
545 17. A. D. Sharrocks, The ETS-domain transcription factor family. *Nat. Rev. Mol. Cell Biol.* **2**,
546 827–837 (2001).
547 18. P. Lemaire, Unfolding a chordate developmental program, one cell at a time: Invariant cell
548 lineages, short-range inductions and evolutionary plasticity in ascidians. *Dev. Biol.* **332**, 48–60
549 (2009).

19. B. Davidson, W. Shi, J. Beh, L. Christiaen, M. Levine, FGF signaling delineates the cardiac progenitor field in the simple chordate, Ciona intestinalis. *Genes Dev.* **20**, 2728–2738 (2006).

20. T. B. Gainous, E. Wagner, M. Levine, Diverse ETS transcription factors mediate FGF signaling in the Ciona anterior neural plate. *Dev. Biol.* **399**, 218–225 (2015).

21. K. S. Imai, K. Hino, K. Yagi, N. Satoh, Y. Satou, Gene expression profiles of transcription factors and signaling molecules in the ascidian embryo: Towards a comprehensive understanding of gene networks. *Development* **131**, 4047–4058 (2004).

22. D. Liu, E. Pavlopoulos, W. Modi, N. Moschonas, G. Mavrothalassitis, ERF: Genomic organization, chromosomal localization and promoter analysis of the human and mouse genes. *Oncogene* **14**, 1445–1451 (1997).

23. L. le Gallic, D. Sgouras, G. Beal, G. Mavrothalassitis, Transcriptional Repressor ERF Is a Ras/Mitogen-Activated Protein Kinase Target That Regulates Cellular Proliferation. *Mol. Cell. Biol.* **19**, 4121–4133 (1999).

24. S. R. F. Twigg, *et al.*, Reduced dosage of ERF causes complex craniosynostosis in humans and mice and links ERK1/2 signaling to regulation of osteogenesis. *Nat. Genet.* **45**, 308–313 (2013).

25. K. Luck, *et al.*, A reference map of the human binary protein interactome. *Nature* **580**, 402–408 (2020).

26. Y. Goyal, *et al.*, Divergent effects of intrinsically active MEK variants on developmental Ras signaling. *Nat. Genet.* **49**, 465–469 (2017).

27. T. Ikeda, T. Matsuoka, Y. Satou, A time delay gene circuit is required for palp formation in the ascidian embryo. *Dev.* **140**, 4703–4708 (2013).

572 28. K. S. Imai, M. Levine, N. Satoh, Y. Satou, Regulatory blueprint for a chordate embryo.
573 *Science (80-.).* **312**, 1183–1187 (2006).
574 29. E. Wagner, M. Levine, FGF signaling establishes the anterior border of the Ciona neural
575 tube. *Dev.* **139**, 2351–2359 (2012).
576 30. A. G. Goglia, *et al.*, A Live-Cell Screen for Altered Erk Dynamics Reveals Principles of
577 Proliferative Control. *Cell Syst.* **10**, 240-253.e6 (2020).
578 31. T. Hiratsuka, *et al.*, Intercellular propagation of extracellular signal-regulated kinase
579 activation revealed by in vivo imaging of mouse skin. *Elife* **2015**, 1–18 (2015).
580 32. N. Ohta, Y. Satou, Multiple Signaling Pathways Coordinate to Induce a Threshold
581 Response in a Chordate Embryo. *PLoS Genet.* **9** (2013).
582 33. L. Guignard, *et al.*, Contact area-dependent cell communication and the morphological
583 invariance of ascidian embryogenesis. *Science.* **369** (2020).
584 34. W. Shi, M. Levine, Ephrin signaling establishes asymmetric cell fates in an endomesoderm
585 lineage of the Ciona embryo. *Development* **135**, 931–940 (2008).
586 35. N. Haupaix, *et al.*, Ephrin-mediated restriction of ERK1/2 activity delimits the number of
587 pigment cells in the Ciona CNS. *Dev. Biol.* **394**, 170–180 (2014).
588 36. S. E. Keenan, *et al.*, Rapid Dynamics of Signal-Dependent Transcriptional Repression by
589 Capicua. *Dev. Cell* **52**, 794-801.e4 (2020).

590

591